



# Lamb Wave Based Damage Detection in Composite Panel

*B. Janarthan, M. Mitra\* and P.M. Mujumdar*

**Abstract** | This paper presents a Lamb wave based methodology for damage detection using frequency spectra in thin metallic and composite plates and a more realistic structure like stiffened carbon-epoxy composite panel. The stiffened specimen considered encompasses almost all the complexities that may be encountered while implementing a Lamb wave based Structural Health Monitoring (SHM) system for real time applications. The complexities considered include cluttering of wave modes, reflections from the stiffeners and edges, effect of structural in-homogeneity like variable thickness on time of flight and amplitude. Thin Piezoelectric patches operating in  $d_{31}$  modes are used as transducers for Lamb wave generation in pitch catch configuration and excitation of  $A_0$  mode through mode tuning. A Root Mean Square Deviation Damage Index (RMSD DI) based frequency spectra is derived out of the windowed  $A_0$  mode of the Lamb wave response. The efficiency of the DI to predict damage severity is tested experimentally for different specimen with known damage location. To substantiate the experimental results, 2-D finite element (FE) simulation is carried out for different damage geometries.

**Keywords:** Structural Health Monitoring; Composite panel; Stiffened composite panel; Lamb wave; Piezoelectric transducers.

## 1 Introduction

Over the last one decade, substantial research, both experimental and theoretical, has been focused on Lamb wave based damage detection in thin metallic and composite plates. In these damage detection methods information about damage is carried by change in characteristics of an elastic wave due to its interaction with the damage, which is recorded by transducers.

The primary advantage of Lamb wave based technique over conventional non-destructive methods is its ability to scan large area, low attenuation, easy implementation using piezoelectric (Lead Zirconate Titanate—PZT) transducers for online Structural Health Monitoring (SHM). A time domain signal records the propagation history of Lamb waves, providing the most straightforward information, such as existence of various wave modes, propagation velocity, attenuation and dispersion with distance, scattering from a

structural boundary or damage.<sup>1</sup> Su et al<sup>2</sup> provided a comprehensive review on the state of the art Lamb wave-based damage identification approaches for composite structures.

However, multi-modal characteristics, dispersive nature and relatively higher speeds of Lamb waves pose a number of challenges in implementing an SHM with Lamb waves. These complexities have restricted the implementation of Lamb wave based SHM mainly to isotropic or composite plates of simple geometries, relatively larger in dimensions and without many discontinuities like presence of stiffeners and joints. Most of the existing works on Lamb waves have used changes in the amplitude, time of flight and time reversal of wave packets, to identify damage in both isotropic and composite plates where the  $S_0/A_0$  modes are well separated without cluttering and without merging of waves due to edge reflections. This is possible only in structures which

are of sufficiently large dimensions without any discontinuities in the path of the wave propagation.

Real life aerospace structures however, have higher complexities in terms of stiffeners, joints, variable thickness and other discontinuities. Compared to the extensive work done on Lamb wave based damage detection in flat metallic/composite panels, similar studies for stiffened panels are very few to the best of authors' knowledge. Studies conducted on the interaction of Lamb wave with geometric discontinuities<sup>3</sup> show the complexities involved quite clearly in a stiffened plate, revealing that the interaction of zero order anti-symmetric guided Lamb mode ( $A_0$ ) with a structural discontinuity in a composite structure undergoes mode-conversion.

Chetwynd et al.,<sup>4</sup> undertook a case study of damage detection in a curved carbon-fibre reinforced panel with two omega stiffeners. Outlier analysis was used to undertake conversion of a windowed averaged time domain signal into scalars for damage detection, which was later used for analysis in multilayer perceptron neural network for localization of damage. Lu et al.<sup>5</sup> studied propagation characteristics of Lamb waves in a carbon fibre/epoxy (CF/EP) composite stiffened panel sufficiently large (900 mm × 560 mm) with five stiffeners spaced 80 mm equally lengthwise indicating wave attenuation with propagation distance, cluttering of modes, signal complexities and wave energy loss across reinforced stiffeners. Considering the complexities of the time domain data, an inverse algorithm based on correlation between wave signals (both  $A_0$  and  $S_0$ ) obtained in pristine and damaged structures (with a through thickness hole) was developed. Park et al.<sup>6</sup> undertook a comparative study of various Damage Index (DI) algorithms based on Lamb waves to test sensitivity to damages like loosen bolts and delamination in a composite stiffened panel with two bolted stiffeners and two bonded stiffeners. The study compared Active Damage Interrogation (ADI), Time Domain RMS (TDRMS), Short Time Fourier transform (STFT) and Time Reversal (TR) DI algorithms for damage detection. Monnier<sup>7</sup> proposed a percentage damage index using frequency response of Lamb waves to identify delamination due to impact loads on a slightly curved Carbon Fiber Reinforced Plastic (CFRP) stiffened panel. The experimental study indicated the potential of frequency spectra in damage detection.

This paper presents the applicability of a Root Mean Square Deviation Damage Index (RMSD DI) based on frequency domain data to large flat isotropic plates, Glass Fiber Reinforced Plastic (GFRP) plates and also to a realistic and relatively smaller dimension stiffened CFRP plates for damage

detection. Lamb waves are generated and recorded using PZT patches as transducers. Only  $A_0$  Lamb wave mode is excited through mode tuning. The RMSD DI is derived from the frequency spectra of windowed  $A_0$  mode of the Lamb wave response for isotropic and composites. Extensive theoretical and experimental work is carried out to appreciate the sensitivity of the  $A_0$  mode for damage detection. Finally, the complete procedure of deriving the DI from a raw time domain signal was automated for detection of known stiffener debonding damages.

The paper is organized in three sections; section 2 explains the complete experimental setup, introducing all the specimen, signal for interrogation and the hardware units used for the experiment. The following sections deals with the brief introduction of simulation technique used for isotropic and composite materials and also introduces to various 2D Finite Element (FE) models used for analysis. Third section deals with the results and analysis drawn from both experiments and simulation. Finally, the paper ends with important conclusions.

## 2 Experimental Setup

### 2.1 Signal generation and acquisition

First, Lamb wave is generated and recorded using PZT transducers in flat aluminium, flat composite and stiffened composite panels. The complete experimental set-up and process is described in this subsection. PZT transducers type SP-5 A (7 mm × 5 mm × 0.48 mm) and type SP-5H (5 mm × 5 mm × 0.25 mm) are used. The PZT transducers are fixed to the structure using a thin layer of Araldite®, two component epoxy resin paste adhesive of high strength and toughness. Three different materials are used in this work, namely, AL 5052 aluminium alloy, E-glass/Ly556 (GFRP) and T300/914 (CFRP). The complete experimental and simulation work is conducted in pitch catch configuration. As actuators, they have a high piezoelectric-mechanical coupling effectiveness (the maximum strain that can be transmitted to the substructure) and high maximum allowable electric field (to avoid de-poling, which would destroy the piezoelectric properties).<sup>4</sup> As sensors, they have a very high operating frequency (>10 kHz), making them suitable for the sensing of dynamic force events. Moreover, they offer a high resolution.<sup>4</sup> After initial trials carried out by earlier students investigating the time reversibility of Lamb-waves,<sup>5</sup> various parameters related to such experimentation have been optimized and 7 mm PZT patches were selected. The Hanning window modulated eight cycle tone burst signal (Fig. 1) is used to excite the PZT actuators by a Tektronix AFG3021B multifunction generator. The eight cycle tone burst signal is generated using Tektronix

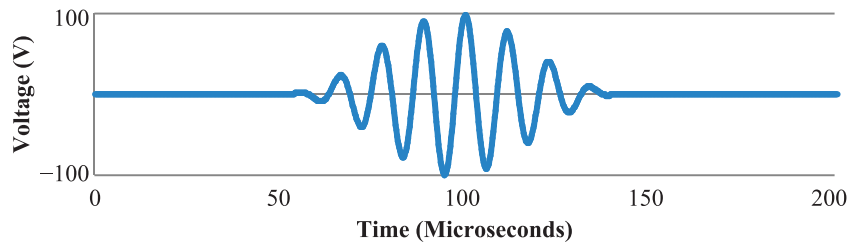


**Figure 1:** Hanning window modulated 8 cycle tone burst input signal.

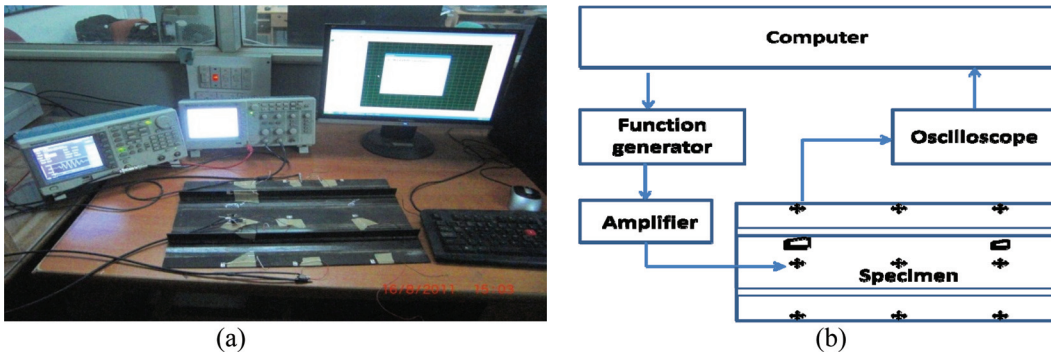


**Figure 2:** (a) Experimental setup with the CFRP stiffened plate (b) schematic diagram of the setup.

Arbexpress-AXW100©. The Lamb wave response is acquired from the PZT sensors through a Tektronix TDS 1002B two channel oscilloscope which involve 2500 discrete data point. To avoid aliasing, acquisition is undertaken at a sampling rate of 5 mega samples per second. To reduce the effects of high frequency electro-magnetic noise, the recorded signals are filtered using a low pass eighth order Butterworth filter. The experimental setup and schematic of the setup is shown in Fig. 2(a) and (b).

## 2.2 Experimental specimens

Three test specimens namely; aluminium plate, GFRP plate and CFRP stiffened plate are used for the experiment. The details of these specimens are presented in the following sub section.

**2.2.1 AL 5052 specimen:** The dimension of the AL 5052 plate used is  $1.5 \text{ m} \times 1.5 \text{ m} \times 1.6 \text{ mm}$ . The choice of a large plate is only to prevent edge reflections contaminating the Lamb wave signals and cluttering the  $A_0$  and  $S_0$  modes. Lamb wave responses are recorded for four different types of damages induced in the plate. The schematic diagram of the specimen with the position of the sensors is shown in Fig. 3. The different damages introduced in the plate are shown in Fig. 4(a), (b) and (c). The dimensions and location of the damage with respect to sensor/actuator is given in Table 1. PZT patch of type SP-5H is used to undertake the

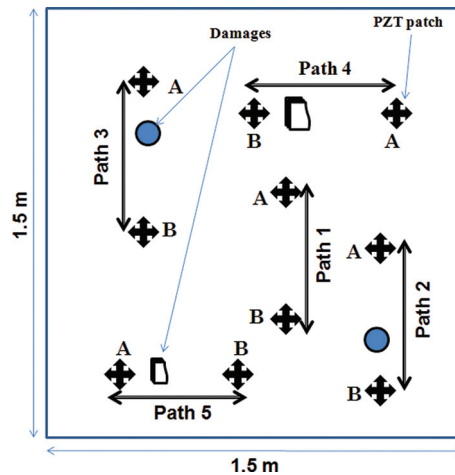


**Figure 3:** Schematic of transducer configuration.

experiment. The actuator and the sensor are separated by a distance of 26.2 cm to see that  $A_0$  and  $S_0$  modes are not cluttered at the sensor location.

**2.2.2 E-Glass/Ly556 (GFRP) specimen:** This specimen contains 5 layers of woven fabric lamina made of E-Glass fibers and Ly556 resin. The dimension of the plate is  $1 \text{ m} \times 1 \text{ m} \times 2.205 \text{ mm}$  (Fig. 5(a)). PZT patches type SP-5A are fixed at a separation distance of 20 cm along the zero fiber direction to obtain wave speed along the fiber direction and another pair of sensors are placed

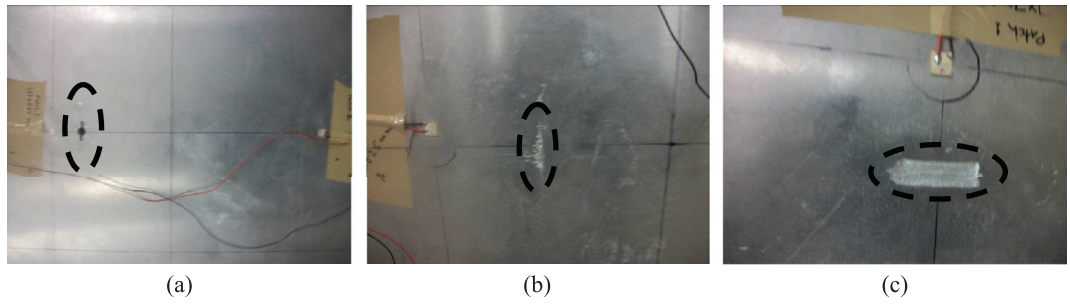


**Figure 4:** (a) Through thickness damage (b) notch damage (c) surface damage.

**Table 1:** Introduced damage dimensions and location in AL 5052 specimen.

	Damage dimensions in-between the actuator sensor path	Location of damage from position B (cm)
<b>Path 1</b>	No damage	–
<b>Path 2</b>	8 mm diameter through hole	18.9
<b>Path 3</b>	Through hole with a 2 cm rectangular hole across the circular hole	2.25
<b>Path 4</b>	About 0.0008 deep damage through thickness	21.20
<b>Path 5</b>	7 cm Wide and about 0.0008 m deep damage along the surface	3.00

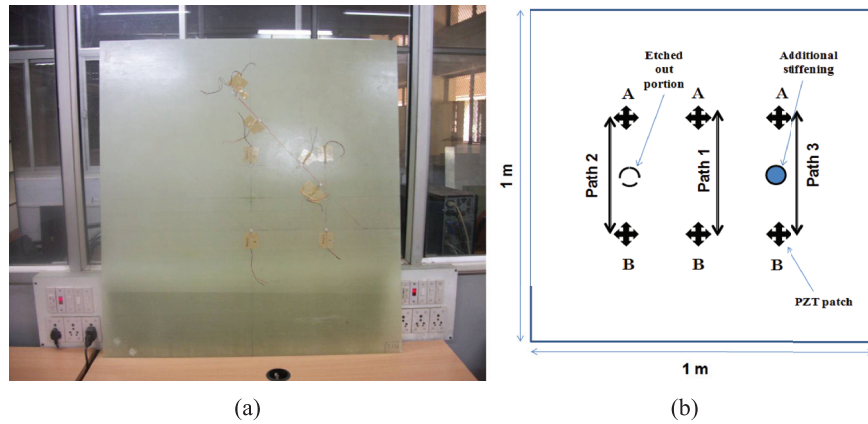


**Figure 5:** (a) E-Glass/Ly556 specimen (b) schematic of transducers in GFRP plate.

at a separation distance of 32.5 cm at a measured angle of 45° to the 0° fiber direction by aligning the longer side of the PZT at an angle 45° to the 0° fiber. Lamb wave responses are picked up along three different paths with 20 cm distance between actuator and sensor (schematic shown in Fig. 5(b)). The details of the transducer configuration are tabulated in Table 2.

**2.2.3 T300/914 (CFRP) stiffened aircraft plate specimen:** The stiffened composite panel is shown in Fig. 6(a). It is made from T300/914 carbon epoxy pre-preg. The panel dimensions are

450 mm × 300 mm × 2.4 mm with two stiffeners placed symmetrically with respect to the centerline 150 mm apart along the longer side of the plate. As mentioned earlier, the specimen exhibits several complexities of an aircraft composite panel; the smaller size of the plate brings in wave merging and interference with edge reflections. The base plate has a 16 layer symmetric layup sequence  $[45/-45/0/45/0/-45/0/90]_s$  and the T-stiffeners layup is  $[45/-45/0/45/0/-45/0/90]$  placed back to back. PZT patches of type SP-5A are used as transducers.

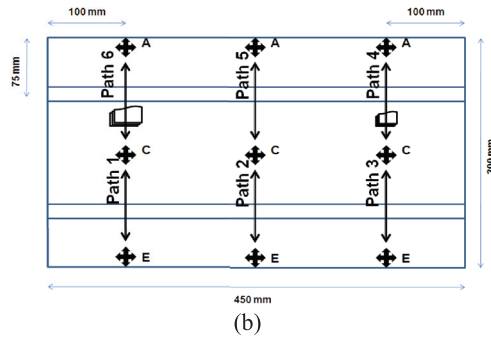
The CFRP composite panel contains two small regions of stiffener de-bonding approximately 2 cm<sup>2</sup>

**Table 2:** Introduced damage dimensions and location in GFRP specimen.

	Introduced change in-between the actuator sensor path	Location from position B (cm)
<b>Path 1</b>	No damage/additional stiffening along zero fiber direction	–
<b>Path 2</b>	1" circular disc etched out to half depth of the plate to reduce stiffness	10
<b>Path 3</b>	Additional stiffening by gluing of a 1" circular disc so that the thickness of the plate is doubled in that location	10



(a)



(b)

**Figure 6:** (a) Carbon-epoxy stiffened panel specimen (b) transducer positions and damage location.

and 1 cm<sup>2</sup>, at the inner edge of one of the stiffener flange, as shown in Fig. 6(a) (hash marking) and 6(b). Nine active PZT patches are bonded at the locations shown in Figure 6(b), forming six wave propagation paths across the stiffeners. Two of these actuator-sensor paths pass through the de-bond regions in the specimen. The sensors at 'A' and 'E' are deliberately positioned very close to the edge of the plate to avoid complications arising from longer edge reflections. The test is conducted at a central frequency of 92 and 100 kHz with an 8 cycle tone burst signal shown in Fig. 1. To minimize the complexities of Lamb wave as mentioned earlier, only  $A_0$  mode is excited through mode tuning. Mode tuning is achieved by fixing two PZT patches on either surfaces of the structure at the same location. The PZT patches are then excited out-of-phase to generate enhanced  $A_0$  mode.

### 3 Finite Element (FE) Models

In this section, the 2D FE models are developed to simulate Lamb wave responses of the experimental specimens are presented.

#### 3.1 FE model for AL 5052 plate

The FE model is done using ANSYS 13© under plane strain conditions. The structural 2D model is built for analysis with free-free boundary conditions.<sup>9</sup> The thickness plane along the wave propagation path is meshed along eight noded plane 183 elements. New mark's time integration scheme

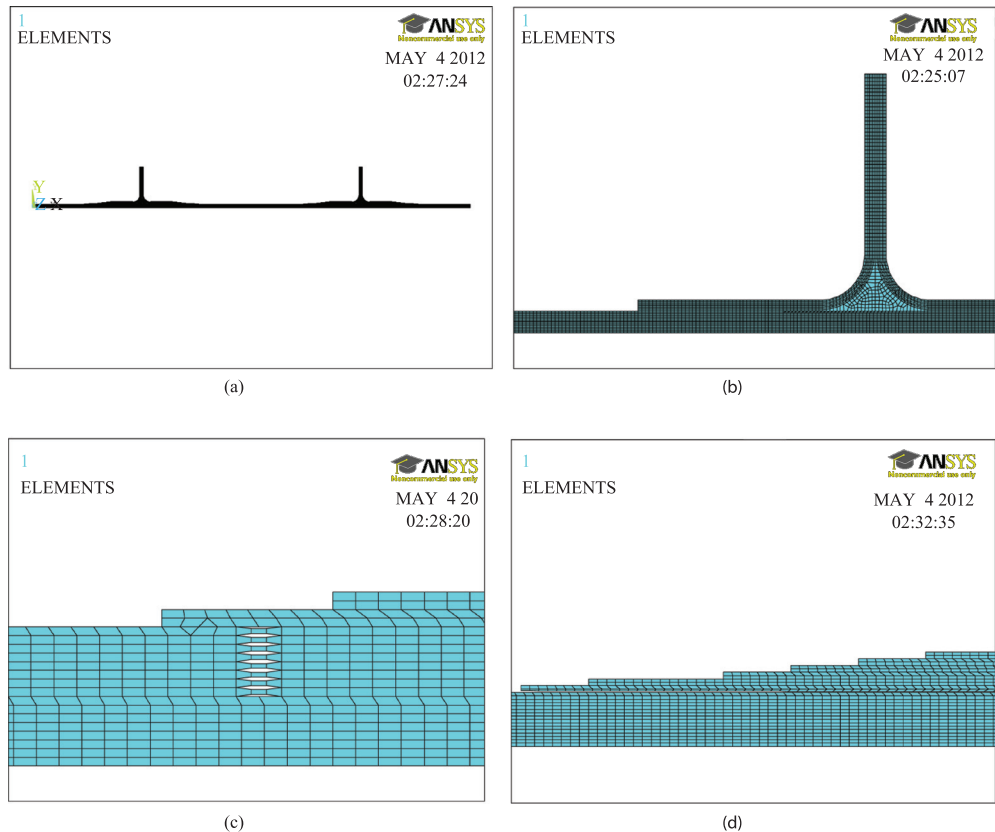
is used for analysis with a time interval of 2  $\mu$ s. A pin force model is used for simulating actuation and sensing. The cross sectional dimension of the plate is 1.25 m  $\times$  1.6 mm. The material properties assigned to the model is same as that of the experimental specimen (Young's modulus—70.3GPa, Poisson's ratio—0.33 and density—2680 Kg/Cm<sup>3</sup>). A finer meshing using an element size of 0.4 mm (12500 elements) was chosen to capture the Lamb wave speeds accurately through convergence study with different element sizes. Simulation technique is validated by verifying wave speeds obtained by Lamb wave experiment. V grooves of different depth and rectangular grooves with same depth but different length in the line of path of the Lamb waves are also modeled (Table 3).

#### 3.2 E-Glass/Ly556 (GFRP) plate

For the composite laminate, layer wise cross sectional modeling of GFRP composite along thickness (0.2205 mm each layer) and lateral dimension (1.25 m) is done. Hence, the material properties of every layer as per the orientation of the fiber are obtained along 1 and 3 directions<sup>10</sup> for assigning material property (same as that of the experimental specimen) in ANSYS©. The transversely isotropic property of the unidirectional lamina of E-glass/Ly556 is 55 GPa ( $E_{11}$ ). The cross sectional dimension of the plate is 1.25 m  $\times$  1 GPa ( $E_{22}$ ), 5.5 GPa ( $G_{12}$ ), 4.6 GPa ( $G_{23}$ ), 0.3( $\nu_{12}$ ) and 0.37( $\nu_{32}$ ).

**Table 3:** Geometric discontinuities dimensions and location in a 2D AL 50502 plate model (total of 10 models).

0.0005 m wide V-groove depth located at 10 cm from excitation node	0.0008 m deep Rectangular groove width located at 10 cm from excitation node
0.0004	0.0005
0.0008	0.001
0.00012	0.0015

**Figure 7:** 2D FE model of the CFRP stiffened test specimen (a) with ply drop (b) without ply drop (c) 8 ply delamination with ply drop (d) stiffener de-bonding with ply drop.

### 3.3 T300/914 (CFRP) stiffened aircraft plate

Next, the stiffened composite panel is also modeled in the same proven and tested method used for GFRP plate. In the stiffened plate, in addition to the presence of stiffener, the ply drops in the specimen which come in to existence due to the technique of attaching stiffeners to the base plate adds to the complexities. Hence, multiple reflections from the edges of the ply drop make analysis of the Lamb waves more difficult. Thus, understanding of the Lamb wave propagation in stiffened panel is important before undertaking damage detection experiments. A thickness wise cross sectional 2D FE model similar to the specimen is modeled both

with and without stiffener. The stiffness matrices for the said orientation is obtained using the transversely isotropic material properties (130 GPa ( $E_{11}$ ), 10 GPa ( $E_{22}$ ), 5 GPa ( $G_{12}$ ), 4.1 GPa ( $G_{23}$ ),  $0.35(v_{12})$ ,  $0.44(v_{32})$ ) and density value is calculated by method of mixture as  $1580 \text{ Kg/m}^3$ .

Stiffened plate models with different stiffener configuration and the actual specimen configuration were modeled to understand the characteristics of wave propagation in such panels. T-stiffeners with ply drop and without ply drop are modeled to analyze the effect of ply drop on Lamb wave propagation (Fig. 7(a) and (b)). Similarly, various degrees of delamination<sup>11</sup> and debonding are also modeled in base plate configuration and in the

**Table 4:** Models for various extents of delamination and de-bonding in CFRP stiffened model.

Degree	CFRP base plate	CFRP stiffened plate			
	Smaller delamination (0.4 mm)	Larger delamination (0.8 mm)	Smaller delamination (0.4 mm)	Stiffener de-bonding	
	Position from actuator (mm)	Position from actuator (mm)		Depth of de-bonding (mm)	
				Position from actuator (mm)	
8 Ply	37.5	37.5		20	35.8
6 Ply	37.5	37.5		40	35.8
2 Ply	37.5	37.5		–	

specimen stiffened plate configuration with ply drop (Fig. 7(c) and (d)) to understand the changes induced in the frequency spectra of the Lamb wave responses. Simulation undertaken for various degrees of stiffener de-bonding and delamination as relevant to this work is presented in Table 4.

## 4 Results and Analysis

### 4.1 Generation of Lamb waves

First, the PZT patch on a pristine AL 5052 plate is excited with a 100 kHz 8 cycle tone burst signal as shown in Fig. 1 and the recorded wave speeds are verified with the dispersion plot of aluminium. These speeds are also validated with the obtained experimental wave speeds. Similar experiment is conducted on the GFRP plate. The wave speeds of the  $A_0$  and  $S_0$  calculated from the experimental and simulation Lamb wave responses are tabulated in Table 5. The wave speeds obtained through FE simulation for Al 5052 Aluminium alloy plate and the composite laminates  $[0/90]_5$  and  $[45/-45]_5$  are found to be in good agreement with the experimental results.

### 4.2 AL 5052 aluminium alloy

**4.2.1 Formulation of damage index:** As explained before, the initial experiments are conducted on plates of AL 5052 and GFRP plates with large dimension to obtain separated  $A_0$  and  $S_0$  can be obtained. Lamb wave responses are recorded with a 100 kHz tone burst signal along 5 paths depicted in Fig. 2 of the AL 5052 specimen. The Lamb wave responses of path 1 (pristine state) and path 5 (Fig. 3) are shown in Fig. 8(a).

The response through the damage indicates change in the Time of Flight (ToF) of both  $S_0$  and  $A_0$  modes and considerable dispersion in the  $A_0$  mode. The dispersion plot indicates that  $A_0$  wave speed vary steeply in comparison to  $S_0$  at 0.16 MHz-mm (Fig. 8(b)). Thus,  $A_0$  is more affected from any change in the thickness of the structure at lower frequency ranges. In addition, at low operating frequencies the amplitude of  $S_0$

is too small and is prone to faster attenuation than  $A_0$ . Hence, when  $A_0$  interacts with the change in the thickness of the plate due to the introduction of damage, it incurs equivalent change in the frequency spectra of the Lamb wave response. The dispersed  $A_0$  indicates considerable modulation due to interaction with the damage thus change in the frequency content of the modes. In case of complex geometries obtaining local time domain information like ToF, amplitude variation may not be possible due to complexities explained before. Thus, understanding the change in the frequency content of the signals may help in identifying damage. Initially this study is done for a specimen with an easier geometry and isotropic material. This would later help in developing the method for a more complex structure like CFRP stiffened plate.

The idea behind this work is to obtain an index that can identify and quantify the damage facilitating automation and in-situ SHM for real life structural components. The RMSD Damage Index (DI) is used as a damage indicator. The expression for the RMSD DI used in this work is given below,

$$DI_{RMSD} = \sqrt{\frac{\left(\sum_{i=1}^n (x_i - y_i)^2\right)}{\left(\sum_{i=1}^n (y_i)^2\right)}} \quad (1)$$

where,  $x_i$  and  $y_i$  are the magnitude of the  $i$ th spectral line of the Discrete Fourier Transform (DFT) at the frequency resolution chosen to compute the DFT i.e. Fourier coefficients of the time domain data of interest for damaged and undamaged conditions respectively,  $n$  is number of sample points. The discrete time domain data is transferred to a frequency domain using the inbuilt FFT algorithm of MATLAB. The function `fft(X,n)` returns the  $n$ -point DFT of vector  $X$  (in this case a matrix in MATLAB), computed with a Fast Fourier Transform (FFT) algorithm. The DI is measured considering the magnitude of the  $i$ th spectral line of the discrete Fourier transform in a frequency

**Table 5:** Wave speeds of  $A_0$  and  $S_0$  in E-Glass/Ly556 (GFRP) composite.

S No	Stacking sequence	$S_0$ Wave speed		$A_0$ Wave speed	
		Simulation	Experiment	Simulation	Experiment
1	$[0/90]_5$	4084 m/s	4123 m/s	1382 m/s	1408 m/s
2	$[45/-45]_5$	3416 m/s	3462 m/s	1363 m/s	1387 m/s

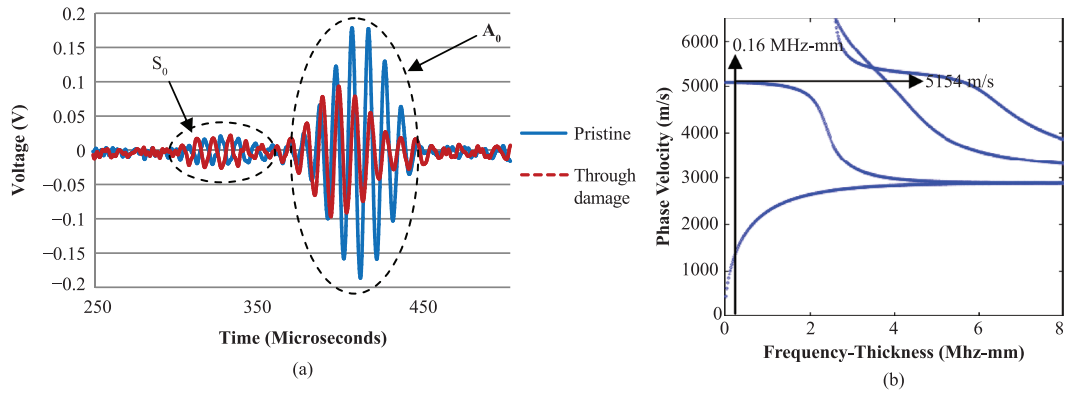


**Figure 8:** (a) Lamb wave response in Al 5052 plate for path 1 (pristine) and path 5 (through damage) (b) dispersion plot for aluminium showing experimentally obtained wave speeds.

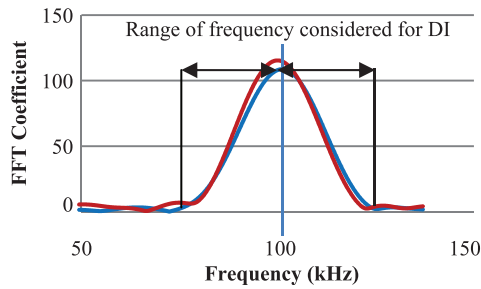


**Figure 9:** Frequency spectra of two single tone burst signal of a Lamb wave response depicting the methodology of calculating DI.

range across the central frequency spread equally as shown in Fig. 9. The DI is a measure of the similarity between the two frequency spectra in terms of the error between the damaged and undamaged signal.<sup>5,18</sup> Thus, it gives the overall difference between the frequencies spectra’s of two signals.

**4.2.2 Damage index for experimental Lamb wave responses:** The frequency domain based DI given by Eqn, 14 is implemented to experimentally obtained Lamb wave responses for the aluminium plate for simplicity. Here, first the reflected wave packets present in the Lamb wave responses are truncated and only the  $A_0$  and  $S_0$  modes are transformed into the frequency domain using FFT. The frequency spectrum of the signals between a pair of transducers with damage in the

wave path as shown in Fig. 2 are compared with response from path 1 containing no damage (Path 1), which is taken as the baseline. The frequency spectra response for responses along paths 4 and 5 obtained in the experiment in comparison with the baseline is shown in Fig. 10. The RMSD DI applied to the frequency spectra of different Lamb wave responses through damage are tabulated in Table 6.

Calculated RMSD DI shows consistent increase in their value with respect to the severity of the damage, except for path 2. This discrepancy can be attributed to the poor directivity of the actuator. It should be mentioned here that the DI calculated among Lamb wave responses for different undamaged paths vary with a maximum value of 0.15 which is mostly due to the minute in-homogeneity and slight thickness variation.

**4.2.3 Damage Index for simulated Lamb wave responses:** To ascertain the validity of the DI, various damage models as tabulated in Table 3 are used for obtaining simulated Lamb wave responses. The frequency spectra of the Lamb wave responses with various damage models are shown in comparison with the frequency spectra of the undamaged plate is shown in Figs. 11 and 12.

The DI values obtained for various damage geometries are tabulated in Table 7. The DI values

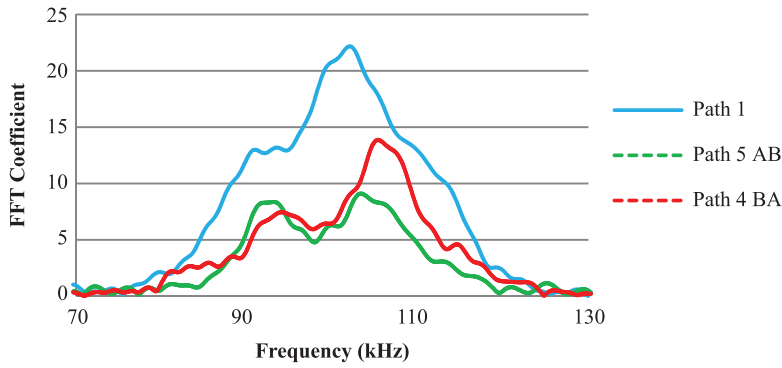


**Figure 10:** Comparison of the frequency spectra of Lamb wave responses with deep through thickness damage near sensor A (path 4) and wide and deep through thickness damage near sensor B (path 5).

**Table 6:** Calculated DI for experimental Lamb wave responses through different damages in AL 5052 plate.

	Wide and deep damage (Path 5)	Deep damage (Path 4)	Rectangular damage through thickness (Path 3)	Circular damage through thickness (Path 2)
<b>DI Value</b>	0.566756	0.639893	0.977767	0.383945

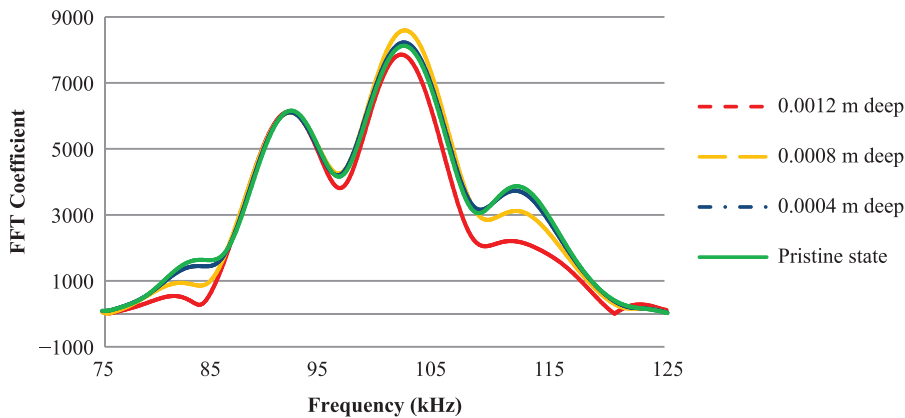


**Figure 11:** Frequency spectra of Lamb waves responses through a V-groove (Table 3) in comparison with pristine state.

show a similar increasing trend with the severity of the damage, both in thickness and surface length of the damage. Experimental and simulation DI was calculated for a similar V-groove geometry which is 1 mm in width and 0.6 mm and the obtained DI values are 0.06339 and 0.05587 respectively. The difference in the DI obtained with experiment and simulation for a similar model may be attributed to several uncertain factors like geometric inhomogeneity, electromagnetic noise, transducer bonding differences etc indicating the simulation conditions offer ideal state free from signal contamination and geometric inhomogeneity.

#### 4.3 E-Glass/Ly556 (GFRP) composite

First, to understand the influence of the damage on the Lamb wave responses in the GFRP laminate the experimental responses along the three different paths shown in Fig. 5(b) are recorded and are presented in Fig. 13. The change in the stiffness due to the damage show considerable variation in the wave speeds and also in the amplitudes of  $A_0$  and  $S_0$ . Amplitude decreases for reduction of stiffness in  $A_0$  mode while it increases in  $S_0$  mode and the vice versa effect takes place in case of increase in stiffness. However, the magnitude of variation is grossly different and greater influence is seen in  $A_0$  mode than in  $S_0$  mode for both the cases.

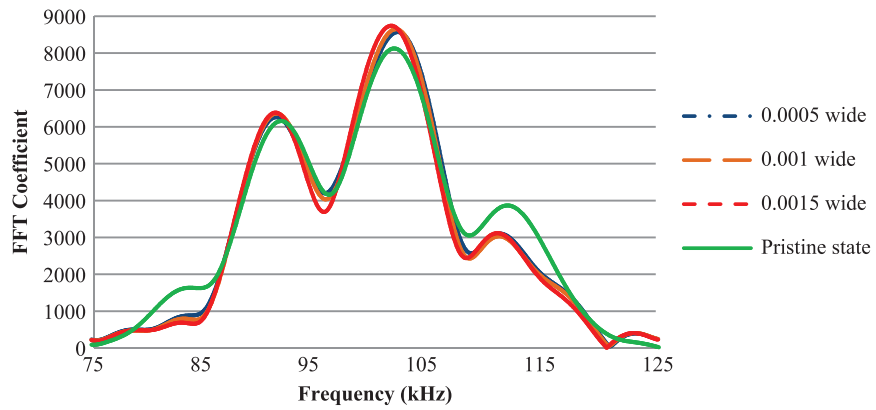


**Figure 12:** Frequency spectra of Lamb waves responses through rectangular groove (Table 3) in comparison with pristine state.

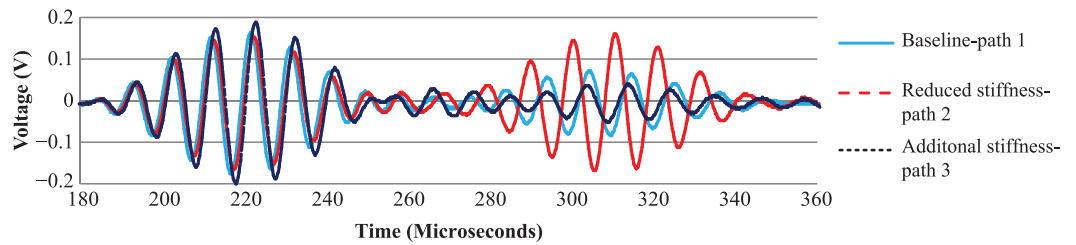


**Figure 13:** Comparison of experimental Lamb wave response between path 1 (Baseline), path 2 (with reduced stiffness) and path 3 (with additional stiffening).

**Table 7:** DI values for simulated Lamb wave responses through different damage geometries in AL 5052 plate.

0.0005 m wide V-groove depth	DI value	0.0008 m deep rectangular groove width	DI value
<b>0.0004</b>	0.023602	<b>0.0005</b>	0.106789
<b>0.0008</b>	0.086284	<b>0.001</b>	0.117172
<b>0.00012</b>	0.170786	<b>0.0015</b>	0.132938

Next, neglecting the reflection wave packets, only the  $A_0$  and  $S_0$  are transformed into frequency domain using FFT and shown in Fig. 14(a). The DI is calculated with reference to path 1 (Fig. 4(b)) considering it as the base line. The obtained values are shown in Table 8. The FFT pattern is different from those seen for Al 5052 plates. The path reversal DI shows a low DI value of 0.016 indicating in-homogeneity in the structure as can be seen from Fig. 13(b). One more interesting observation is that frequency spectra of Lamb wave propagation along 45° path is considerably different from that along the 0° fiber direction (Fig. 14(b)). In addition, the DI value obtained for the lamb

**Table 8:** DI values for experimental Lamb wave responses in GFRP plate.

	Path 1 reverse	Additional stiffness path 3	Reduced stiffness path 2	45 deg path
<b>RMSD DI Values</b>	0.016419	0.770869	0.271742	0.825263

wave responses in reversed path 1 is much lower than that obtained for the response along 45° path. This shows the limitation arising due to directionality when Lamb waves are used for damage detection by this method.

**4.4 Need for mode selection**

The following inferences can be drawn and summarized from the obtained Lamb wave responses, frequency spectra and calculated DI based on the frequency spectra through experiments and simulations undertaken in AL 5052 Aluminium alloy and GFRP plate specimens,

- At low frequencies amplitude of  $S_0$  is too low in AL 5052 and hence significant loss in signal strength is seen in pitch catch configuration.

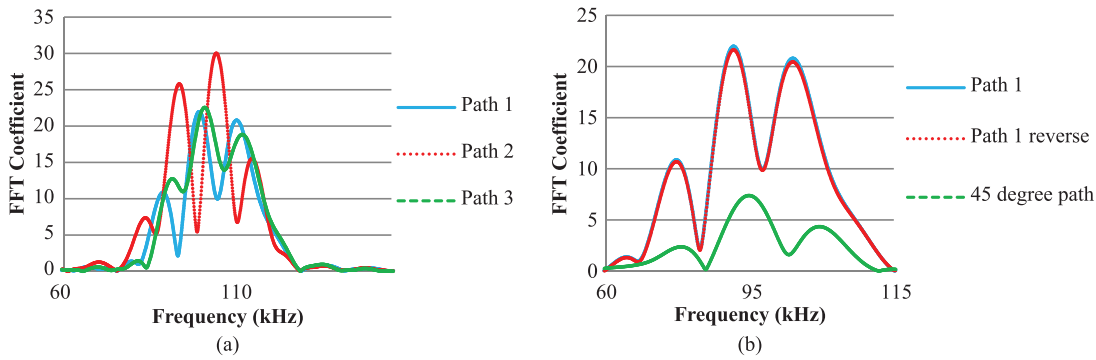


**Figure 14:** Comparison of the frequency spectra (a) for varying stiffness (b) for different wave propagation direction.

- $A_0$  mode signal is highly dispersive at low operating frequencies exhibiting better potential to identify damage through frequency spectra.
- DI values calculated by comparing Lamb wave response of a undamaged path with the response recorded in the same path but in reverse direction gives a maximum value of 0.158 for Al 5052 and 0.016 for a GFRP plate. This indicates that setting up a threshold is necessary to automate this technique.
- FFT pattern is not consistent for the same central frequency in different media under inspection. This is largely due to the influence of the varying amplitude and dispersion characteristics of  $A_0$  and  $S_0$  in different media.
- DI value shows consistent increase in the value with the severity of the damage even when both the  $A_0$  and  $S_0$  are considered. However, better patterns can be worked out, when considering specific modes with better sensitivity.

**4.5 Selection of specific mode for damage identification**

**4.5.1 Mode selection for AL 5052 specimen:** It has been observed that  $A_0$  mode is influenced more by the presence of a damage in the wave path. Thus,  $A_0$  mode is considered to show better response in the frequency spectra. Further, the amplitude dispersion plot<sup>1</sup> for a 1.6 mm thick aluminium plate indicate amplitude of  $S_0$  modes is too low in comparison to  $A_0$  mode till about 200 kHz. Thus, the weak signal strength of  $S_0$  at such low frequency makes the usage of  $S_0$  mode for damage detection in Al 5052 plates ineffective. This inference is confirmed by the DI values calculated for both experimental and simulated responses by transforming the individual  $A_0$  and  $S_0$  independently to frequency domain. The results are tabulated in Tables 9, 10 and 11. The frequency

**Table 9:** DI values for individual  $A_0$  and  $S_0$  obtained from the simulated Lamb wave responses considering rectangular grooves in AL 5052 plate.

		Mode	0.0005	0.001	0.0015
<b>RMSD DI Values</b>	$S_0$		0.082003	0.095604	0.103057
	$A_0$		0.070466	0.078352	0.101032

**Table 10:** DI values for individual  $A_0$  and  $S_0$  obtained from the simulated Lamb wave responses considering V-grooves in AL 5052 plate.

		Mode	0.0012	0.0008	0.0004
<b>RMSD DI Values</b>	$S_0$		0.118795	0.053157	0.012319
	$A_0$		0.134818	0.062595	0.031867

**Table 11:** DI values for  $A_0$  mode obtained from experimental Lamb wave responses for damages in AL 5052 plate.

		Mode	Deep damage (path 4)	Wide and deep damage (path 5)
<b>RMSD DI Values</b>	$A_0$		0.04811	0.087578

spectra of  $A_0$  mode alone is presented in Fig. 15. The calculated DI value shows consistent increase in the value with severity of the damage. The FFT pattern seems to be simpler and qualitative assessment of damage can be made easily even before calculating the damage index.

**4.5.2 Mode selection for GFRP/composites specimen:** Similar analysis is performed for the GFRP laminate.  $A_0$  and  $S_0$  modes are separately

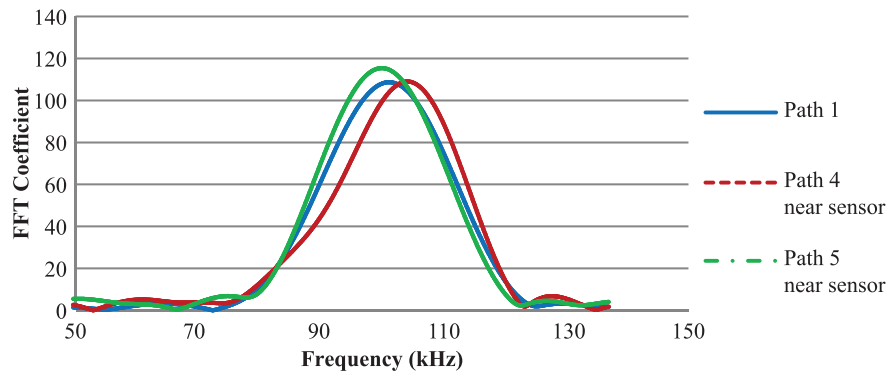


**Figure 15:** Frequency spectra of  $A_0$  mode signal along path 1, 4 and 5 in AL 5052 plate with the damage near sensor.

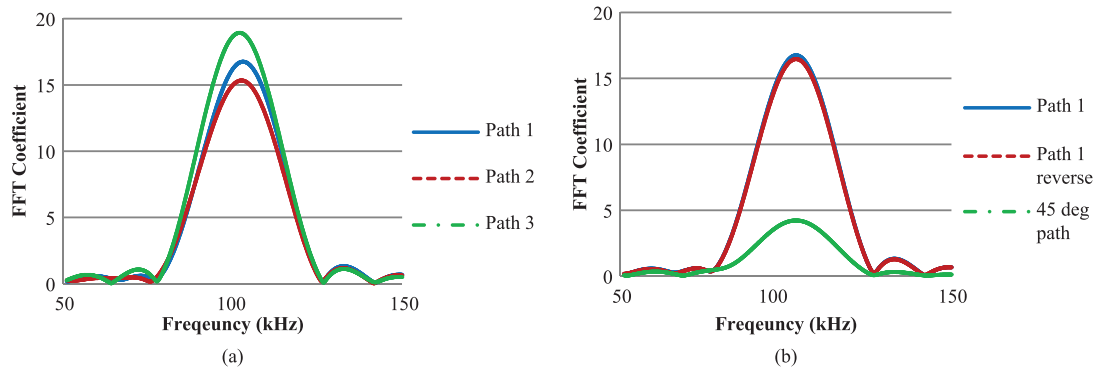


**Figure 16:** (a) Comparison of the frequency spectra of  $S_0$  mode showing variation with damage (b) comparison of frequency spectra of  $S_0$  mode showing variation with direction of wave propagation.

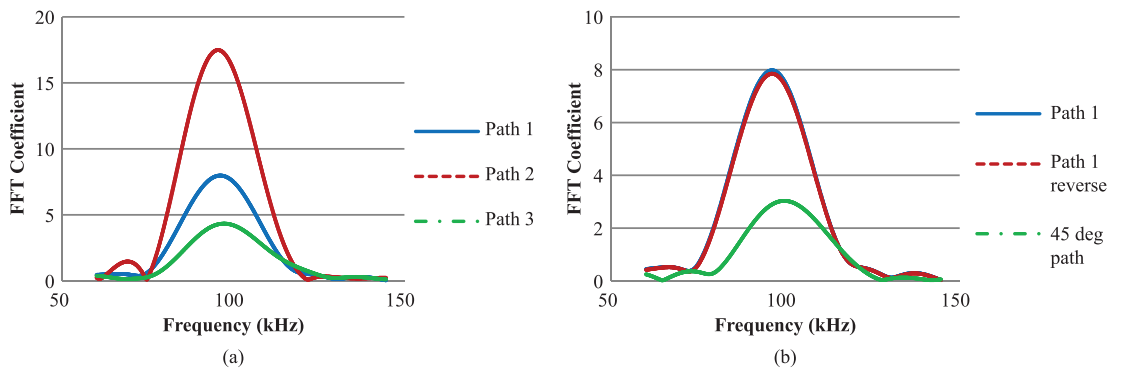


**Figure 17:** (a) Comparison of the frequency spectra of  $A_0$  mode showing variation with stiffness (b) comparison of frequency spectra of  $A_0$  mode showing variation with direction of wave propagation.

extracted from the time domain data recorded in all the three paths with varying stiffness, in  $45^\circ$  fiber direction and in reverse direction of path 1 (baseline), transferred to frequency domain are presented in Figs. 16(a) and (b) for experimental responses and Figs. 17(a) and (b) for simulated responses. The DI values are calculated for

all the responses in comparison with the base line to ascertain that  $A_0$  shows better response than  $S_0$  for stiffness variation. The obtained DI values are shown in Table 12. Frequency spectra change by the direction of Lamb wave propagation is also captured to a closer magnitude unlike when both modes are used in combination.

**Table 12:** DI values for individual  $A_0$  and  $S_0$  obtained from the experimental Lamb wave responses with stiffness variation in GFRP plate.

	Mode	Path 1 reverse	Additional stiffness path 3	Reduced stiffness path 2	45 deg path
<b>RMSD DI Values</b>	$A_0$	0.016082	0.443732	1.15456	0.609135
	$S_0$	0.017007	0.149569	0.078644	0.748617

#### 4.6 Inferences from the results for AL 5052 and GFRP plates

The following inferences can be drawn from the responses, frequency spectra and calculated DI based on the frequency spectra presented in the last sub-section,

- $A_0$  mode responds better to change in the stiffness, thickness and density at low frequencies than  $S_0$ . Thus, it would be able to identify damages like through thickness damages in isotropic plates, delamination and stiffener deboning in composites as these damages bring about gross changes in the stiffness of the structure. This is clearly brought about by the DI values found by experiment and simulation for AL 5052 and GFRP plates.
- Lamb wave characteristics like wave speed, amplitude etc and even frequency spectra varies with fiber orientation. Thus, Lamb wave characteristics remain same only when the Lamb wave propagation w.r.t fiber direction remains same. This indicates that stiffeners have much less effect on the Lamb waves than the fibre lay-up.
- Lower threshold value is achieved with  $A_0$  mode in comparison with  $S_0$  mode.

#### 4.7 T300/914 (CFRP) stiffened composite—experiment and simulation

**4.7.1 Influence of stiffener on Lamb wave propagation:** Figure 18 presents the Lamb wave response from stiffened panel compared to that of the base plate without stiffener. The response is obtained at a node 0.3 m from the excitation node. The Lamb wave responses obtained show shift in the peak amplitude of the  $A_0$  mode and high distortion of  $S_0$ . Thus, identifying  $A_0$  and  $S_0$  merely by ToF from the dispersion plot is incorrect.

As the plate dimension along the wave propagation direction is 300 mm, adequate time is not available for the  $A_0$  and  $S_0$  modes to separate out completely. Therefore,  $A_0$ ,  $S_0$  and the edge reflections tend to clutter with each other for both the

clean base plate and stiffened plate. In addition, for the stiffened plate, the  $S_0$  mode and the edge reflections are distorted substantially due to the presence of additional wave packets from the stiffener. Thus, presence of a stiffener in the path of the Lamb wave shows additional wave forms reflected from the stiffener end, rejoining the wave propagating through the base plate, modulating the response and transforming the characteristics. Thus, it can be observed from Figs. 19(a) and (b) that in addition to the distortion due to merging of reflections from edges, the presence of stiffeners distorts the time domain Lamb wave responses to a large extent, and presence of waves resulting from damage if any will be camouflaged by the reflections from the stiffeners.

The second observation from this and similar experimental results is that the presence of stiffener strongly attenuates the amplitude of  $S_0$  mode unlike  $A_0$  mode amplitude. Figure 20 shows comparison of Lamb wave responses recorded along path 1 and 6 (Fig. 6(b)) by inducing excitation at transducer E and capturing responses experimentally at transducer C and A, one after first stiffener and the other after both stiffeners.

The response clearly indicates step by step reduction in the amplitude of  $A_0$  signal across each stiffener. Hence, adequate amplification of the signal is required for analysis. The presence ply drop is also a characteristic feature of composite stiffeners. The presence of ply drop reduces the change in the wave speed but reduces the stiffener spacing and hence mode cluttering is bound to happen as evident from the Fig. 21 in comparison with the plate with a stiffener without ply drop.

The reference from the Lamb wave responses can be summarized as follows,

- The presence of stiffeners results in several reflected waves which clutter  $A_0$  and  $S_0$  and can hide the waves arising from the damage.
- The amplitude of  $S_0$  is drastically reduced as it travels through the stiffener.
- Spacing between stiffeners considerably affects mode separation and ply drop reduces the spacing and hence increases mode cluttering.

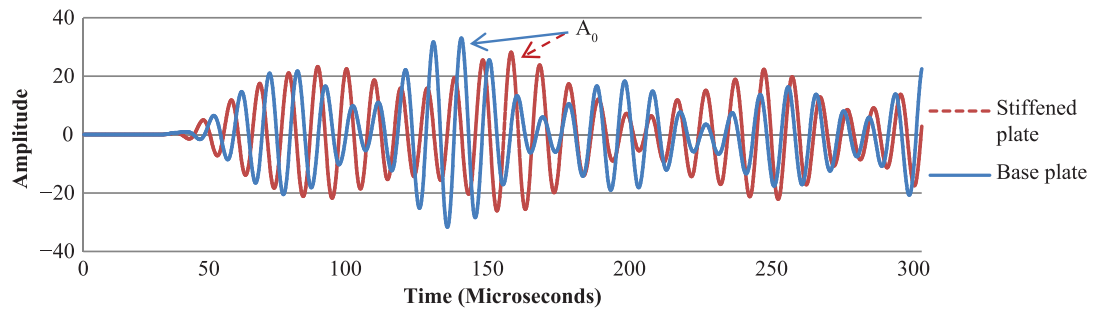


**Figure 18:** Comparison of simulated Lamb wave response on a base plate and stiffened plate model.

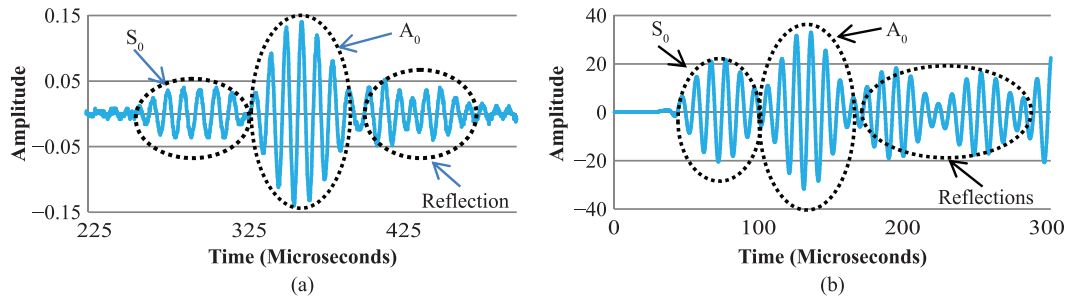


**Figure 19:** (a) Experimental Lamb wave response of path 3 in stiffened plate (b) simulated Lamb wave response on a similar clean base plate without stiffener.

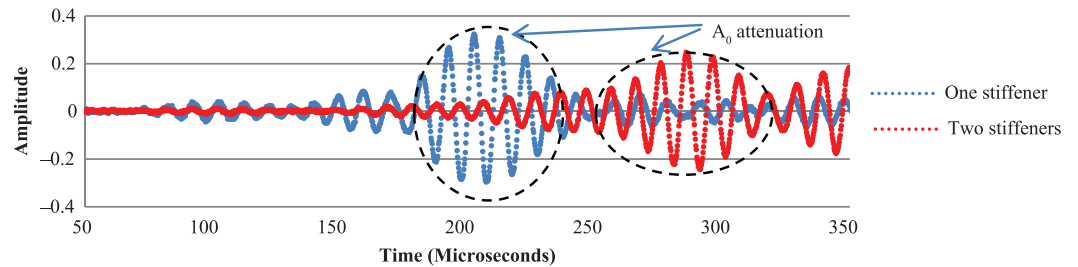


**Figure 20:** Experimental Lamb wave response showing attenuation of  $A_0$  mode after one and both the stiffeners.

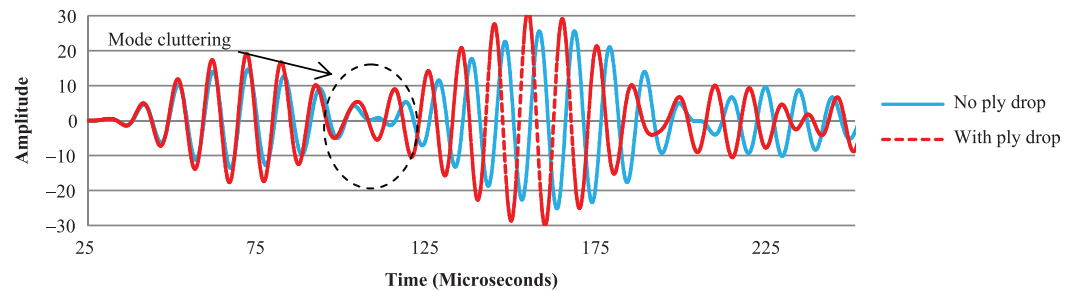


**Figure 21:** Comparison of simulated Lamb wave response for a stiffened plate with and without ply drop.

- Identifying  $S_0/A_0$  mode with wave speed is not possible as the wave speed varies considerably due to the inherent complexities. Hence,

a mode selection approach is adopted wherein a desired mode can be enhanced and the other unwanted modes can be suppressed.

#### 4.7.2 Mode tuning experiments—time domain analysis:

Considering the reasons deliberated and reasoned out from earlier experiments, it is opined that tracking  $A_0$  mode would be appropriate to extract features for damage detection. Both the  $S_0$  and  $A_0$  mode are sensitive to structural damage, however,  $A_0$  mode shows higher sensitivity to surface damage.<sup>1</sup> Thus,  $A_0$  mode is considered more suitable for identifying de-bonding on the surface of the CFRP base plate. Mode tuning experiment is conducted on the stiffened panel with  $A_0$  tuning setup. PZT patches are placed one over the other in location A and C in all the six actuator—sensor paths (Fig. 6(b)). Fig. 22 presents the tuned and untuned Lamb wave response of the stiffened panel. It can be seen that the  $A_0$  mode is enhanced substantially with  $S_0$  being reduced.

**4.7.3 Damage assessment for simulated responses:** The complete methodology of extracting desired mode, converting to frequency

domain and calculating DI is automated through MATLAB® guide feature (Fig. 23).

ANSYS® simulation of Lamb wave responses for various degrees of delamination and de-bonding of the stiffener are recorded for an excitation of 100 kHz. Later the DI values calculated by transforming the  $A_0$  mode from the complete signal are tabulated in Table 13. The frequency spectra of the windowed  $A_0$  of the simulated Lamb wave response for various degrees of delamination and debonding are shown in Fig. 24.

Further, for the same degree of delamination the DI value obtained is lower for a stiffened pane in comparison to a clean base plate without stiffener (Fig. 25). This is because the  $A_0$  mode extracted from the original response contains some portion of unidentified mode coupled with it. Simulated Lamb wave responses for de-bonding of the stiffener shows that the Lamb wave response gradually moves towards base plate configuration with increase in the length of de-bond along the

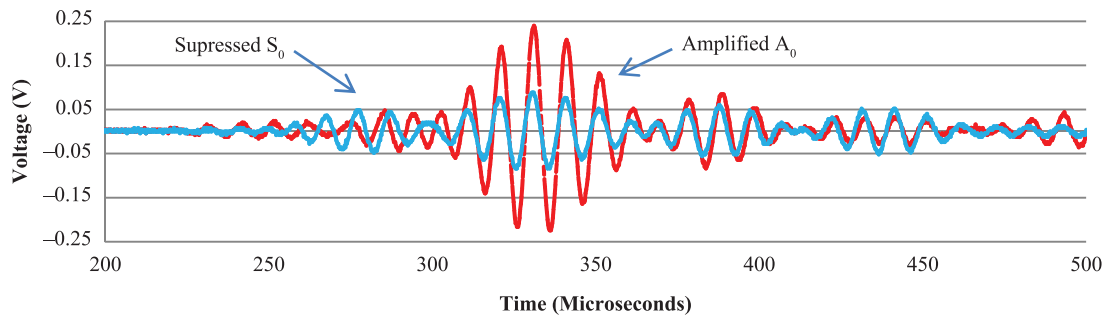


Figure 22: Comparison of tuned and un-tuned Lamb wave response along path 2.

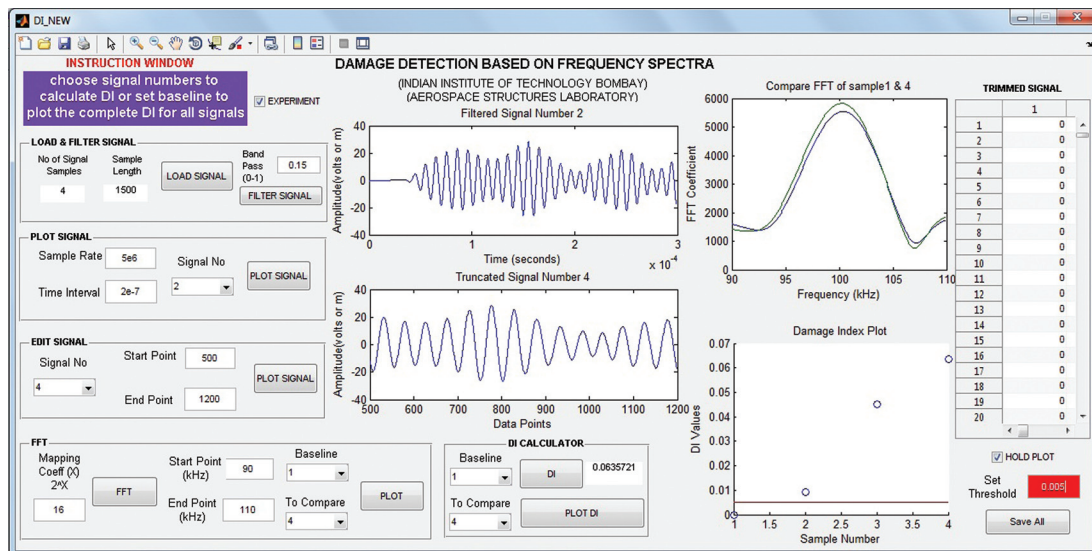
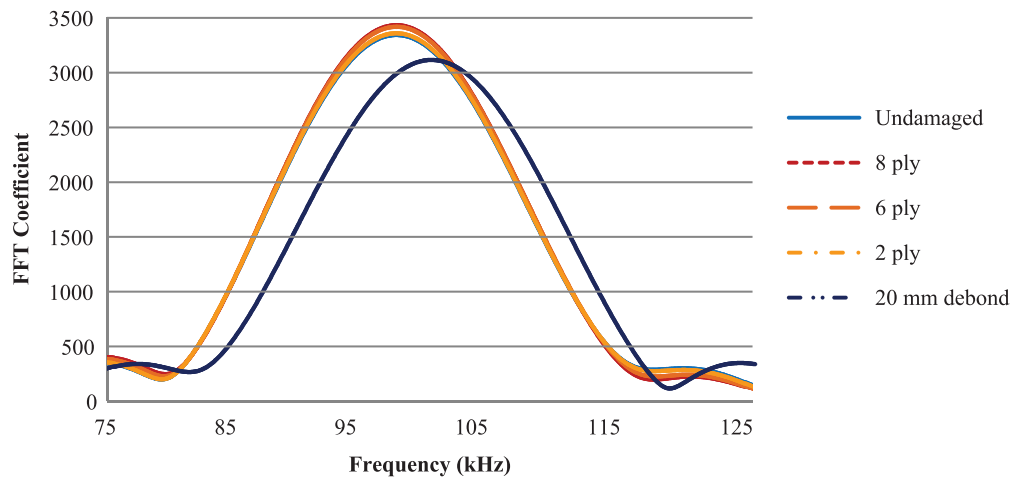


Figure 23: GUI of the application automating the methodology for damage detection.

**Table 13:** DI values for simulation responses of various degrees of delamination and de-bonding in CFRP base plate and CFRP stiffened plate model.

Degree	CFRP base plate		CFRP stiffened plate		
	Smaller delamination (0.4 mm)	Larger delamination (0.8 mm)	Smaller delamination (0.4 mm)	Stiffener de-bonding	
	Position from actuator (37.5 mm)	Position from actuator (37.5 mm)	Position from actuator (37.5 mm)	Depth of de-bonding (mm)	Position from actuator (35.8 mm)
<b>8 Ply</b>	0.0172	0.0325	0.0113	20	0.3068
<b>6 Ply</b>	0.0155	0.026	0.0082	40	–
<b>2 Ply</b>	0.0145	0.00576	0.0017	–	–



**Figure 24:** Comparison of FFT of windowed A<sub>0</sub> of simulated Lamb wave responses for various degrees of delamination and 20 mm stiffener de-bond.

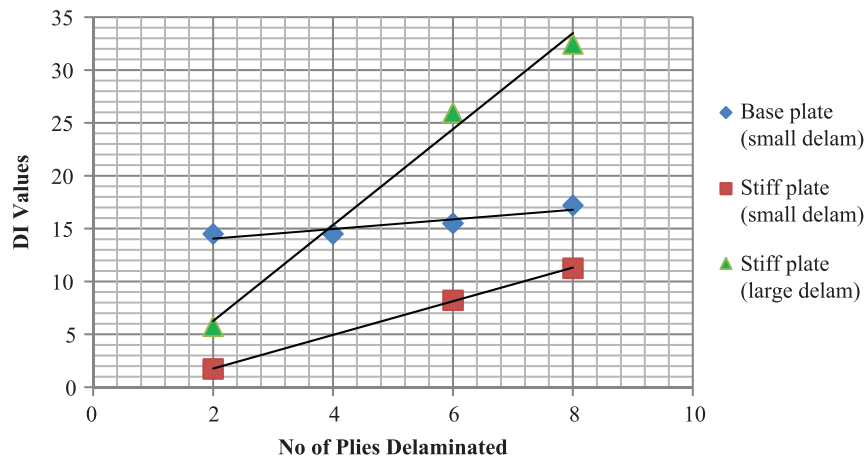


**Figure 25:** Comparison of DI values for various degrees of delamination in CFRP base plate and stiffened plate.

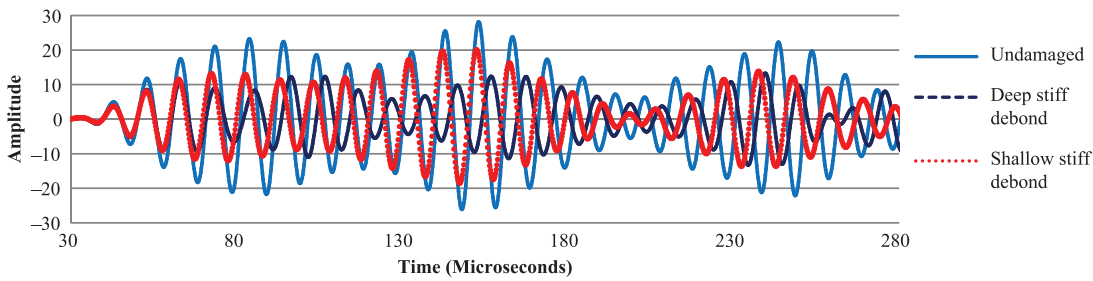


**Figure 26:** Simulated Lamb wave responses comparing pristine state, 20 and 40 mm deep debond.

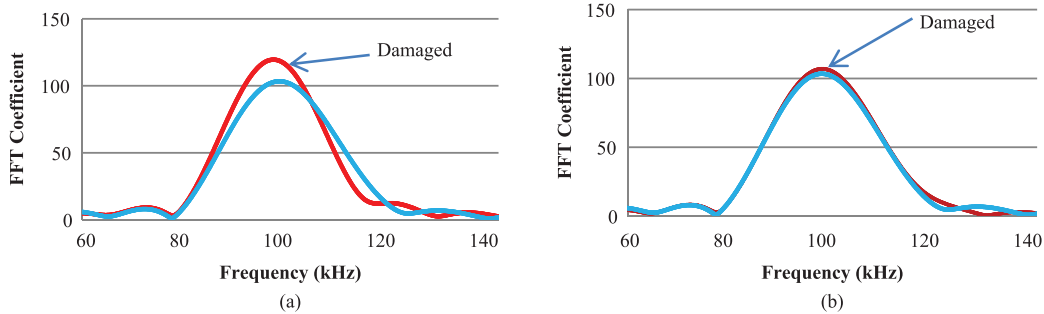


**Figure 27:** Experimental results (a) comparison of  $A_0$  mode frequency spectra of path 2 and 6 (b) comparison of  $A_0$  mode frequency spectra of path 2 and 4.

Lamb wave propagation path. Thus, larger debond (40 mm in depth) along the Lamb wave propagation path tends to distort  $A_0$  even new wave packet is introduced in the response as compared to a smaller debond (Fig. 26).

#### 4.7.4 Frequency domain analysis for damage assessment using experimental responses:

Though, Fig. 22 shows that the tuned Lamb wave response primarily containing  $A_0$  is much clearer with less cluttering, it may not be used directly for damage identification. Unlike the simulated Lamb wave responses, experimental Lamb wave responses are truncated, so that only the predominant  $A_0$  signal responses are considered for transformation into the frequency domain as shown in Fig. 27(a) and (b). This figure shows the comparison of frequency spectra of paths 2 and 6 and paths 2 and 4 at 92 kHz considering only the  $A_0$  mode. Narrowing down to the use of only  $A_0$  mode has brought down the threshold from 0.17 to 0.15 (Fig. 28). The experimental DI values obtained through usage of only  $A_0$  mode clearly indicate the presence of damage in path 4 and 6 and the value difference also indicates the severity of the damage accurately.

Both simulation and experiment indicate the potential of the damage index based on frequency spectra for damage detection. Thus, it is concluded

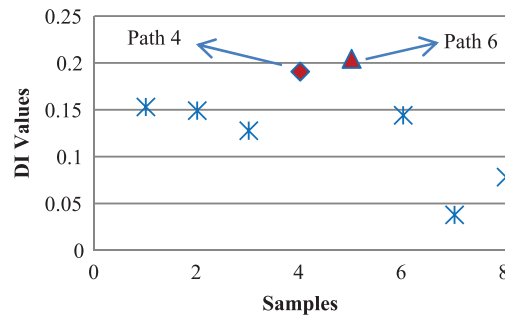


**Figure 28:** DI values obtained experimentally considering  $A_0$  response.

that the damage index works fine in indicating severity of the damage for both thin isotropic and composite plates. The DI is suitable for even complex and realistic structures like a stiffened panel where tested and proven techniques for damage identification in flat structures fail. This paper only indicates the potential of frequency spectra information useful for damage detection. The experiment is conducted in a controlled laboratory environment, hence influence of external factors like temperature is not considered in this work. Simulation requires no threshold selection but due to a number of variables in a real time structure intensive work would be required to

characterize the whole structure under investigation to set up thresholds for implementation of a real time SHM.

## 5 Conclusion

Extensive experimental and simulation study was carried out on different specimens with increasing degree of complexities to namely flat aluminium, GFRP composite plates and CFRP stiffened plates. A numerical measure was formulated and tested on all the Lamb wave responses obtained from the above mentioned specimens to quantify the severity of the damage. Considering the complexities understood from the time domain responses in stiffened structure, the DI was formulated based on frequency spectra and is tested in simple geometries and later extended to real life structures like the stiffened panels. FE models of isotropic and composite plates with various types of damage severity show consistent increase in the DI value. However, number of variables like in-homogeneity in geometry, electromagnetic noise etc makes the implementation of the technique to real time application more challenging. Thus, setting up of thresholds compensating for the in-homogeneities will help in automating the technique for damage detection. A simple guide feature based GUI application is developed using MATLAB® to illustrate the possibility of establishing a real time in-situ SHM system. Both experimental and simulation results show promising results depicting possibility of establishing a real time SHM for complex thin walled composite structures.

Received 1 September 2013.

## References

1. Z Su and L Ye, "Identification of Damage Using Lamb Waves From Fundamentals to Applications", Springer 2009, e-ISBN: 978-1-84882-784-4.
2. Z Su, L Ye and Y Lu, "Guided Lamb waves for identification of damage in composite structures: A review", Laboratory of Smart Materials and Structures (LSMS), Centre

for Advanced Materials Technology (CAMT), School of Aerospace, Mechanical and Mechatronic Engineering, The University of Sydney, NSW 2006, 20 March 2006.

3. C Ramadas, Krishnan Balasubramaniam, M Joshi and CV Krishnamurthy, "Interaction of Lamb mode ( $A_0$ ) with Structural Discontinuity and Generation of "Turning modes" in a T-joint", 2011 Elsevier.
4. D Chetwynd, F Mustapha, K Worden, J A Rongong, S G Pierce and J M Dulieu-Barton, "Damage Localisation in a Stiffened Composite Panel", 2008, Blackwell Publishing Ltd.
5. Y Lu, L Ye, D Wang, Z Zhong and I Herszberg, "Damage Detection in a Large Composite Panel of Five Stiffeners Using Lamb Wave Signals", Materials forum volume 33 (2009).
6. C Y Park, "Damage Index Comparison for a Composite Stiffened Panel Using Lamb Wave", Advanced Materials Research Vols. 26–28 (2007).
7. T Monnier, "Lamb Waves-based Impact Damage Monitoring of a Stiffened Aircraft Panel using Piezoelectric Transducers", Journal of Intelligent Material Systems and Structures 2006.
8. B Janarthan, M Mitra and P M Mujumdar, "Damage Detection in Stiffened Composite Panel using Lamb Waves", EWSHM, July (2012).
9. S Sorohan, N Constantin, M Găvan and V Anghel, "Extraction of Dispersion Curves for Waves Propagating in Free Complex Waveguides by Standard Finite Element Codes", Ultrasonics 51 (2011).
10. J N Reddy, "Mechanics of Laminated composites plates and shells", second edition, CRC press, (2004).
11. Z Su and L Ye, "Lamb Wave-based Quantitative Identification of Delamination in CF/EP Composite Structures Using Artificial Neural Algorithm", Composite Structures 66 (2004).
12. B Poddar, A Kumar, M Mitra and P M Mujumdar, "Time reversibility of a Lamb Wave for Damage Detection in a Metallic Plate", Smart Materials. Struct. 20 (2011) 025001 (10pp) 6 January 2011.



**Squadron leader B. Janarthan** is a commissioned officer in IAF and joined IAF as Undergraduate in Mechanical Engineering during the year 2002. The Officer completed his post-graduation in Aerospace Structures from IIT, Bombay in the year 2012 specializing in the field of structural health monitoring. He started his career as a maintenance engineer with fighter aircraft and its aero engine. During this period the officer has gained practical experience in non-destructive testing of aircraft structures. The officer gained professional experience of instrumentation in aero engine test bed facility and ground testing/characterizing jet aero engines. With this experience, he graduated into manufacture of aircraft/aero engine components and undertaking testing in airborne platforms.



**Prof. Mira Mitra** is currently an Assistant Professor in the Department of Aerospace Engineering at Indian Institute of Technology Bombay, Mumbai, India. She received her Master's Degree and PhD from Indian Institute of Science, Bangalore, India both in Aerospace Engineering. Her research areas include wave propagation, structural health monitoring, composite structures and vibration. She has co-authored 26 Journal papers, 20 conference papers and a book on wavelet methods for dynamical problems with CRC Press. She has received the IEI Young Engineering Award in 2011 and INAE Young Engineer Award in 2010.



**Prof. P.M. Mujumdar** received his BTech, MTech and PhD degrees in Aerospace Engineering from IIT Bombay. His specialization is in the area of Aerospace Structures. He joined the Aerospace Engineering Department of IIT Bombay as a faculty member in 1986. Since then he has been at IIT Bombay, where currently he is Professor and Dean (R&D). His research interests are related to Structural Dynamics, Aeroelasticity & Aeroservoelasticity, Structural & Multidisciplinary Design Optimization, Smart Structures and more recently Structural Health Monitoring.

